Optical and structural study of GaN nanowires grown by catalyst-free molecular beam epitaxy. I. Near-band-edge luminescence and strain effects

Lawrence H. Robins[a)]
National Institute of Standards and Technology, Gaithersburg, Maryland 20899

Kris A. Bertness, Joy M. Barker, Norman A. Sanford, and John B. Schlager
National Institute of Standards and Technology, Boulder, Colorado 80305

(Received 8 May 2006; accepted 28 March 2007; published online 4 June 2007)

GaN nanowires with diameters of 50–250 nm, grown by catalyst-free molecular beam epitaxy, were characterized by photoluminescence (PL) and cathodoluminescence (CL) spectroscopy at temperatures from 3 to 297 K, and high-resolution x-ray diffraction (HRXRD) at ≈297 K. The lattice parameters of the nanowires, determined by HRXRD, are in good agreement with recent measurements of freestanding quasisubstrates; the relative variation of the lattice parameters between the nanowires and quasisubstrates is $\leq 2\times 10^{-4}$. Both as-grown samples, which contained nanowires oriented normal to the substrate as well as a rough, faceted matrix layer, and dispersions of the nanowires onto other substrates, were examined by PL and CL. The D^0X_A line at 3.472 eV, ascribed to excitons bound to shallow donors, was observed in low-temperature PL and CL; free-exciton lines (X_A at ≈3.479 eV, X_B at ≈3.484 eV) were observed in PL at temperatures between 20 and 80 K. The linewidth of the D^0X_A peak was larger in PL spectra of the nanowires than in quasisubstrates. The broadening of the D^0X_A peak in PL of the nanowires is tentatively ascribed to inhomogeneous stress/strain. In addition, the D^0X_A peak was significantly broader in CL than in PL spectra of the same nanowire samples. The further large broadening of the CL peak (as compared to PL) is tentatively ascribed to Stark effect broadening, induced by the electric fields of trapped charges that are created in the CL excitation process.

I. INTRODUCTION

The optical properties of GaN nanowires[1] and related quasi-one-dimensional GaN structures are of great current interest because of the potential applications in light-emitting diodes[2,3], laser diodes,[4] and other photonic devices. Molecular beam epitaxy (MBE) is an attractive growth technology for nanophotonic devices that require material with low impurity and defect content. Well-separated GaN nanowires of good structural quality have been grown[5,6] by catalyst-free MBE, whereas catalyst metal nanoparticles are often required to promote nanowire growth by chemical vapor deposition[2,7–9] (CVD) or physical vapor deposition[10] (PVD). Incorporation of catalyst metal impurities may have detrimental effects on the optical and electronic properties of nanowires grown by the catalyst-assisted methods.

Photoluminescence (PL) and cathodoluminescence (CL) spectroscopies are important techniques for investigation of the electronic structure of wide band gap semiconductors, including intrinsic, impurity, and defect-related states, and the effects of stress/strain, electric fields, or other perturbations. Low-temperature PL and CL measurements often provide more insight into the details of the electronic structure than room-temperature ($T\approx 297$ K in our laboratories) measurements because of broadening and quenching of the emission peaks with increasing temperature. Review articles that discuss PL and CL characterization of GaN and related materials include a general introduction to the growth and properties of III nitride semiconductors by Jain *et al.;*[11] a review of electronic band structure by Vurgaftman and Meyer;[12] and a review of luminescence spectroscopy of defect and impurity states by Reshchikov and Morkoc.[13]

In this study, wurtzite-structure GaN nanowires grown by catalyst-free, nitrogen-plasma-assisted MBE were characterized by PL and CL at temperatures from 3 to 297 K and by high-resolution x-ray diffraction (HRXRD) at room temperature. Growth and structural characterization of these nanowire samples has been discussed previously.[14–16] In this publication (Part I of the present study), the near-band-edge region of the PL or CL spectrum is considered, with peaks ascribed to free and shallow-donor-bound excitons. Strain effects in the nanowires are estimated by comparison to high-quality bulklike samples denoted "quasisubstrates," which are presumed to be nearly strain-free. In a companion article[17] (Part II), lower-energy PL and CL peaks ascribed to defect-related levels are discussed; in addition, CL quenching induced by extended electron-beam irradiation is examined. In both parts of this study, our results are compared to the literature on luminescence spectroscopy of GaN, including studies of MBE-grown nanowires[5,6,18] quasisubstrates,[19–24] and the review by Reshchikov[13] of defect-related luminescence in a range of samples.

II. EXPERIMENTAL PROCEDURE

The nanowire samples examined in this study are designated[14,15] samples B724 and B738. Each sample was grown by catalyst-free, nitrogen-plasma-assisted MBE on an AlN buffer layer on Si(111). Imaging[14,15] by field-emission scanning electron microscopy and dark-field transmission electron microscopy (TEM), showed a rough, faceted, quasi-

[a)]Electronic mail: lawrence.robins@nist.gov

Downloaded 20 Nov 2007 to 132.163.53.194. Redistribution subject to AIP license or copyright; see http://jap.aip.org/jap/copyright.jsp

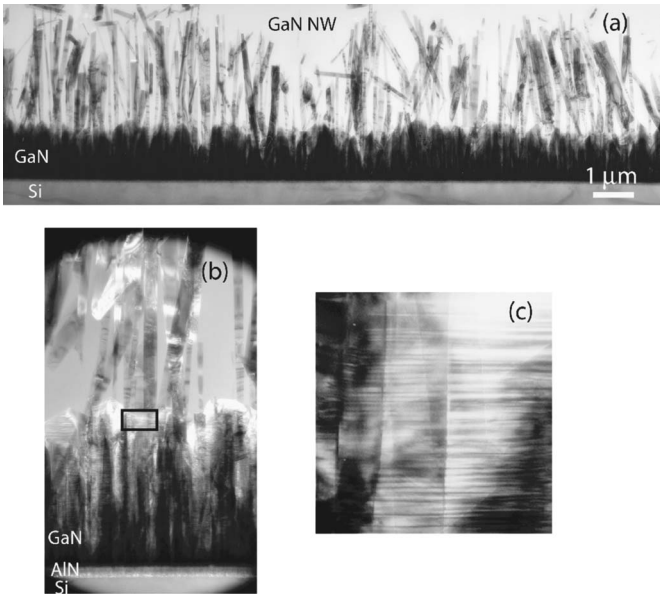

FIG. 1. Dark-field TEM images of nanowires and matrix layer, recorded with a 01−11 reflection strongly excited near the 11−20 orientation, in sample B724. (a) Image of AlN buffer layer, GaN matrix layer, and GaN nanowires demonstrates that most nanowires originate at the AlN surface (suggesting that matrix layer is not essential for nanowire nucleation). (b) Higher magnification view of region inside rectangle in (a) reveals that matrix layer contains a high density of planar defects residing on the basal (0001) planes. (c) Image of portion of single nanowire (above matrix layer) does not show contrast characteristic of planar defects or other extended defects; the bandlike contrast in this image is ascribed to nanowire bending.

continuous "matrix layer" in addition to closely spaced but discrete, approximately vertically growing nanowires. Dark-field TEM images[14] of sample B724, shown in Fig. 1, demonstrate that most nanowires originate at the surface of the AlN buffer layer and extend through the matrix layer. The dark-field TEM images also reveal that the matrix layer contains a high density of planar defects (e.g., stacking faults) residing on (0001) basal planes, which generate diffuse streaking along [0001] in electron diffraction patterns (not shown). TEM images of the upper portions of single nanowires [Fig. 1(c)] do not show features characteristic of planar defects or other extended defects; the light and dark bands seen in Fig. 1(c) are ascribed to bending contrast.

PL and CL measurements of the as-grown samples did not provide sufficient spatial resolution to resolve individual nanowires or distinguish the nanowires from the matrix layer. Therefore, "dispersed" nanowire samples were prepared for optical characterization by ultrasonic agitation of pieces of the as-grown samples in an organic solvent, followed by transfer of the nanowire-solvent mixture to the new substrate.[15] Nanowires were dispersed onto optically transparent sapphire substrates for PL, to enable collection of the emitted light through the substrate, and onto AlGaAs/GaAs, stainless steel, or Si/Ti/Au substrates for CL, to minimize charging effects. Secondary-electron (SE) and CL micrographs of nanowires from sample B738 dispersed on stainless steel are shown in Figs. 2(a) and 2(b), respectively, and SE and CL micrographs of nanowires from sample B738 dispersed on Si/Ti/Au are shown in Figs. 2(c) and 2(d), respectively. The nanowires are highly clustered and, further, are mixed with solvent residue (rounded black spots), in the dispersion on stainless steel, while the nanowires are relatively well-separated and free of visible solvent residue in the dispersion on Si/Ti/Au. (Well-separated nanowires without solvent residue were also observed in a dispersion of sample B724 on stainless steel.) The variation of the morphology of the dispersed samples is not yet understood.

It is presumed that the bottom portions or "roots" of the nanowires mostly remained embedded in the matrix layer during the dispersal processes. Hence, dispersed samples contain primarily the upper portions of the nanowires (as well as some matrix layer and nanowire root material). For examination of the matrix layer and nanowire roots, a sample was prepared by hand polishing of an as-grown sample with 1000 grit SiC powder to remove the top portions of the nanowires, followed by vigorous cleaning to remove any polishing residue.

Lattice parameters of the as-grown samples were measured by x-ray diffraction (XRD) using a triple-axis diffractometer with a 4-bounce Ge(220) monochromator on the incident beam and a Ge analyzer crystal with an acceptance angle of 0.0033°. The c lattice parameter was determined from symmetric reflections at 0002, 0004, and 0006; the a lattice parameter was then determined from asymmetric reflections at 10−14, 10−15, and 20−24.

For variable-temperature PL measurements, samples were mounted in a continuous flow cryostat with temperature control from 3 to 297 K. The as-grown samples [on 0.5 mm thick Si (111) substrates] were clamped securely to a solid copper cold-finger sample holder with beryllium copper spring clips. The dispersed nanowires (on a 0.45 mm thick sapphire substrate) were similarly clamped to a copper sample holder with a 12.5 mm diameter aperture for optical access in transmission. The sample temperature was estimated from measurements with a calibrated rhodium-iron sensor located in the heat exchanger of the cryostat; according to the cryostat specifications, the temperature differential between the sample holder and heat exchanger is ≈ 0.4 K. The sample temperature was not corrected for the possible differential between the heat exchanger and sample surface.

PL was excited by a 325.03 nm (3.813 eV) HeCd laser, chopped at 900 Hz and incident angle (relative to the surface normal) of ≈ 45. The laser intensity incident on the top surface of the sample was $\approx 3\times 10^3$ W/cm^2 for measurements of the as-grown samples and B724 dispersed on sapphire, and 85 W/cm^2 for measurements of B738 dispersed on sapphire. The PL collected from the top surface (for as-grown samples) or through the substrate (for dispersed samples) was spectrally analyzed by a 300 mm monochromator with a 2400 line/mm holographic grating, and slit widths set to 0.10 mm. The PL signal at the monochromator exit slit was detected with a photomultiplier tube and lock-in amplifier. Spectrometer control and data acquisition were computer controlled. The spectrometer wavelength or photon energy calibration was established using spectral lines of the HeCd laser and a Hg/Ar lamp (with absolute wavelengths taken from the NIST atomic spectra database). The energy calibration uncertainty was $\pm 5\times 10^{-4}$ eV from 325 to 546 nm. [Note that all experimental uncertainties in this study repre-

Downloaded 20 Nov 2007 to 132.163.53.194. Redistribution subject to AIP license or copyright; see http://jap.aip.org/jap/copyright.jsp

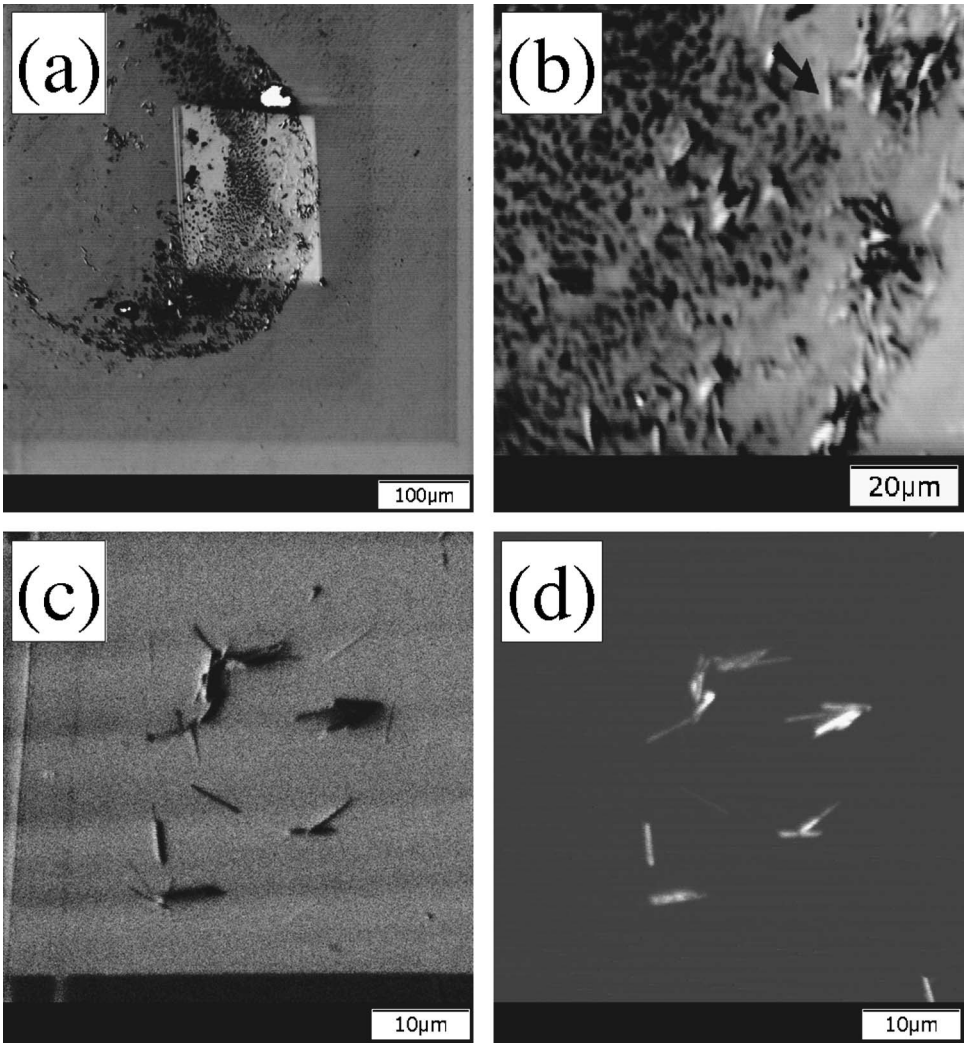

FIG. 2. SE and CL micrographs of nanowires from sample B738, dispersed on stainless steel or on titanium/gold-coated silicon (Si/Ti/Au), taken in the CL/SEM system at $T \approx 15$ K, with experimental conditions as follows: (a) dispersed on stainless steel, SE, beam voltage $=3.14$ kV, current$=21.5$ nA, spot size ≈ 1 μm; (b) dispersed on stainless steel, SE, higher magnification view of a portion of the previous image with the same beam parameters (the slanting arrow near the top indicates a nanowire with approximately vertical image orientation); (c) dispersed on gold-coated Si, SE, beam voltage $=4.89$ keV, current$=8.2$ nA, spot size ≈ 0.4 μm; (d) dispersed on gold-coated Si, CL image of free and donor-bound excitons (3.45–3.50 eV), view of the same area as the previous image with the same beam parameters.

sent 2-standard-deviation (2σ) error bars.] PL spectra were not corrected for the wavelength dependence of the spectrometer response function, whereas such a correction was made for CL.

For CL measurements at ≈ 15 Kor 297 K, samples were mounted with electrically and thermally conductive graphite paste on the cold finger of a liquid-He cold stage in a LaB_6 filament scanning electron microscope (SEM). The sample temperature was estimated from measurements with a calibrated silicon diode sensor embedded in the cold finger. The sample temperature was not corrected for the possible differential between the diode sensor and the sample surface. The SEM beam voltage was 3.14, 4.89, 8.88, or 16.0 kV; according to the Everhart-Hoff model[25,26] of electron-solid interactions, the electron range R (maximum penetration depth) in GaN is 48, 105, 300, and 840 nm, respectively, at these voltages. (Carrier or exciton diffusion effects are not included in the Everhart-Hoff model.) Most CL measurements were done with the following beam settings: either (a) voltage $=3.14$ kV, current$=21.5$ nA, power$=6.8\times 10^{-5}$ W, spot diameter ≈ 1 μm; or (b) voltage$=4.89$ kV, current$=8.2$ nA, power$=4.0\times 10^{-5}$ W, spot diameter ≈ 0.4 μm. The spot diameter (of the focused beam at the sample surface) was estimated from the image resolution. During CL data acquisition, the beam was rastered over a rectangular area between 2.8×10^{-5} and 2.1×10^{-4} cm^2. The peak excitation intensity for CL, calculated from the incident power and focused spot size, was thus 9×10^3 to 3×10^4 W/cm^2, and the time-averaged excitation intensity (over the raster scan period) was 0.19 to 2.4 W/cm^2.

The emitted CL was collimated by mirrors located near the sample, transmitted through a fused-silica window in the SEM, and refocused onto the entrance slit of a 0.34 m spectrograph, with a 600 line/mm grating and entrance slit width of 0.05 mm. The spectra were recorded by a computer-controlled, nitrogen-cooled CCD camera. The wavelength resolution was 0.29 nm, which is equivalent to an energy resolution of $2.3\times 10^{-4}E^2$ eV, where E is photon energy (e.g., the resolution was 2.8×10^{-3} eV at 3.47 eV). The wavelength scale was calibrated with atomic spectral lines, similar to the procedure for PL; the wavelength uncertainty was ± 0.02 nm, which is equivalent to an energy uncertainty of $\pm 1.6\times 10^{-5}E^2$ eV. The CL spectra were corrected for the wavelength-dependent spectrograph response, which was measured with a tungsten-halogen lamp that had previously been calibrated against a NIST standard irradiance source.

Downloaded 20 Nov 2007 to 132.163.53.194. Redistribution subject to AIP license or copyright; see http://jap.aip.org/jap/copyright.jsp

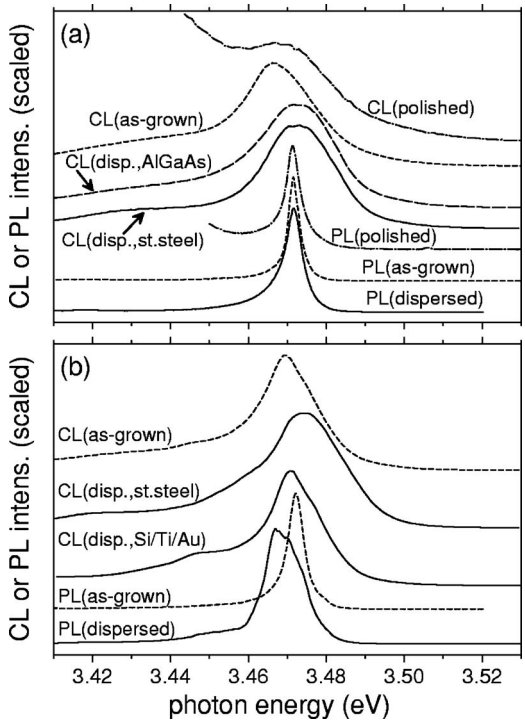

FIG. 3. Low-temperature PL and CL spectra of samples B724 and B738 in the near-band-edge (free-exciton and shallow-donor-bound exciton) region, plotted on linear intensity scales: (a) as-grown, dispersed, and polished pieces of sample B724; (b) as-grown and dispersed pieces of sample B738. PL spectra were acquired at 3 K (polished piece of sample B724) or 10 K (other samples); all CL spectra were acquired at ≈15 K. Incident photon energy for PL spectra was 3.813 eV; incident electron energy for CL spectra was 3.14 keV. Spectra are rescaled to equalize the apparent peak intensities for ease of visual comparison.

III. RESULTS

A. PL and CL spectroscopy

Low-temperature PL and CL spectra of as-grown and dispersed pieces of sample B724 are plotted on a linear scale in the near-band-edge region in Fig. 3(a); similar plots for sample B738 are shown in Fig. 3(b). (Sub-bandgap peaks in the PL and CL spectra are discussed in Part II of this study[17].) The line shapes of most of the PL spectra are slightly asymmetric, with greater broadening on the low-energy side. The CL peaks are significantly broader than the corresponding PL peaks and show more sample-to-sample variation. (In addition, the PL spectrum of sample B738 dispersed on sapphire is broadened and downshifted relative to the other PL spectra.)

Curve-fitting analysis was performed to provide an empirical description of the line shapes of the near-band-edge PL and CL spectra shown in Fig. 3. The fitting function is a sum of Gaussian or hyperbolic secant peaks (note that a hyperbolic secant function has a line shape similar to a Gaussian, but with broader tails). All the PL spectra and most CL spectra were fit with a sum of two peaks. The dominant, higher energy peak is identified as the D^0X_A peak (A exciton bound to a neutral, shallow donor), which occurs at ≈3.472 eV in all PL and CL spectra. The physical origin of the lower-energy peak in the fit, denoted the L peak, is unknown. The L peak may arise from one or more of the following mechanisms: excitons bound to shallow acceptors, bulk defects, or surface states; electron-phonon coupling; inhomogeneous stress/strain; Stark effect due to internal electric fields.

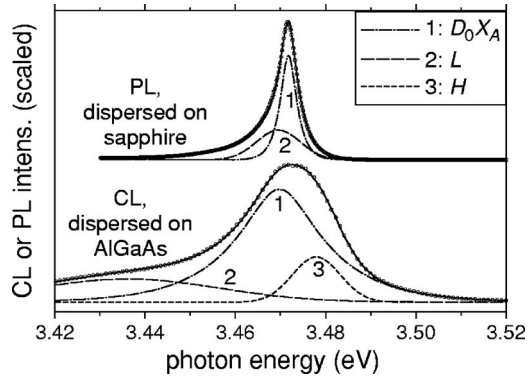

FIG. 4. Low-temperature (10 K) PL spectrum of sample B724 dispersed on sapphire, and low-temperature (≈15 K) CL spectrum of sample B724 dispersed on AlGaAs: data and fitted curves. For each spectrum, the data are plotted as small circles; the overall fitted function is plotted as a solid line; the fitted D^0X_A peak is plotted as a dash-dotted line; the fitted H peak (in the CL spectrum) is plotted as a short-dashed line; and the fitted L peak is plotted as a long-dashed line.

A few CL spectra of dispersed samples could not be fit accurately with a sum of two symmetric peaks. These spectra were fit with a sum of three peaks: the D^0X_A peak, the L peak, and a higher-energy (3.478–3.480 eV) peak denoted the H peak. The physical origin of the H peak is also unknown, and the H peak is poorly resolved from the D^0X_A peak. It should be pointed out that luminescence lines at similar energy to the H peak have been identified in high-quality GaN single crystals:[23,30] D^0X_B (B exciton bound to a neutral, shallow donor) at ≈3.477 eV; X_A (free A exciton) at ≈3.479 eV; and X_B (free B exciton) at ≈3.484 eV. Further, the D^0X_B peak was resolved in low-temperature, linearly polarized PL spectra[27] of single nanowires from sample B738.

Curve-fitting results for the PL spectrum of sample B724 dispersed on sapphire (two-line fit, D^0X_A+L), and the CL spectrum of sample B724 dispersed on AlGaAs (three-line fit, D^0X_A+L+H), are illustrated in Fig. 4. Because of the unknown physical origin of the L and H peaks, and the poor resolution of these peaks from the dominant D^0X_A peak, the L and H peaks will not be discussed further. However, the curve-fitting results will be used to quantify the peak energy (E_{peak}) and full width at half maximum (W) of the D^0X_A peak.

The fitted values of E_{peak} and W for the D^0X_A peak in each low-temperature PL or CL spectrum are listed in Table I. The uncertainties given for E_{peak} and W in Table I were estimated from covariance analysis of the χ^2 function (the sum of squared deviations between the fit and data points). The estimated E_{peak} uncertainties also take into account the photon energy calibration uncertainty of $1.05\times10^{-5}E^2$ (eV units). The curve-fitting results from Table I are represented graphically in Fig. 5. In this figure, the value of E_{peak} for each fitted spectrum is represented by a square symbol, and the vertical bars that encompass E_{peak} represent the interval

Downloaded 20 Nov 2007 to 132.163.53.194. Redistribution subject to AIP license or copyright; see http://jap.aip.org/jap/copyright.jsp

TABLE I. Curve-fitting parameters for the D^0X_A peak (shallow donor-bound A exciton) in near-band-edge PL and CL spectra of GaN nanowire samples, measured at 3–15 K. The fitted peak energy, E_{peak}, and full width at half maximum, W, is listed for each spectrum. Uncertainties (which represent 2σ error bars) in the least significant digits are shown in parentheses; for example, 3.4722(21) eV is read as 3.4722 eV±0.0021 eV.

Sample and measurement	E_{peak} (eV)	W (eV)
B724, as-grown, PL	3.4715(5)	0.0031(1)
B724, dispersed on sapphire, PL	3.4717(5)	0.0042(1)
B724, polished, PL	3.4714(5)	0.0036(1)
B738, as-grown, PL	3.4722(5)	0.0039(1)
B738, dispersed on sapphire, PL	3.4707(6)	0.0104(5)
B724, as-grown, CL	3.4731(8)	0.0186(6)
B724, dispersed on stainless steel, CL	3.4699(5)	0.0134(7)
B724, dispersed on AlGaAs, CL	3.4698(4)	0.0220(4)
B724, polished, CL	3.4713(3)	0.0220(6)
B738, as-grown, CL	3.4711(2)	0.0164(2)
B738, dispersed on stainless steel, CL	3.4722(21)	0.0123(37)
B738, dispersed on Si/Ti/Au, CL	3.4729(2)	0.0153(1)

from $E_{peak}-0.5W$ to $E_{peak}+0.5W$, which can be considered to represent the range of emission energies for an inhomogeneously broadened peak.

Literature results for the D^0X_A energies of quasisubstrate samples grown at Samsung Advanced Institute of Technology[19] (Korea), and at Linköping University [20–23](Sweden) are shown as short vertical bars without central symbols, toward the right-hand side of the graph in Fig. 5. The vertical bars represent the $E_{peak}-0.5W$ to $E_{peak}+0.5W$ ranges for the D^0X_A peaks in the quasisubstrates. The number of resolved D^0X_A peaks in each quasisubstrate sample was one (Ref. 20), two (Refs. 21–23), or three (Ref. 19). In samples where two resolved D^0X_A peaks are observed, the higher-energy peak is ascribed to Si_{Ga} donors and the lower-energy peak is ascribed to O_N donors (see Ref. 19 and references therein).

The temperature dependencies of the near-band-edge PL spectra from sample B724 dispersed on sapphire and sample B738 as-grown are plotted on linear intensity scales in Figs. 6(a) and 6(b). Features on the high-energy side of the D^0X_A peak, which appear either as distinct peaks or "shoulders," are seen to become more prominent with increasing temperature. These features are ascribed to A and B free-exciton (X_A and X_B) recombination, which is expected to become more probable with increasing temperature because of thermal ionization of the shallow donor-bound exciton and thermal population of higher-energy states. Vertical arrows pointing to the X_A and X_B peaks at intermediate temperature (≈50 K), are shown in Fig. 6. The X_A and X_B peaks were best resolved for the as-grown piece of sample B738. The peak widths are seen to increase with increasing temperature. Because of the thermal broadening, the excitonic peaks become unresolved at temperatures of 80 K or higher.

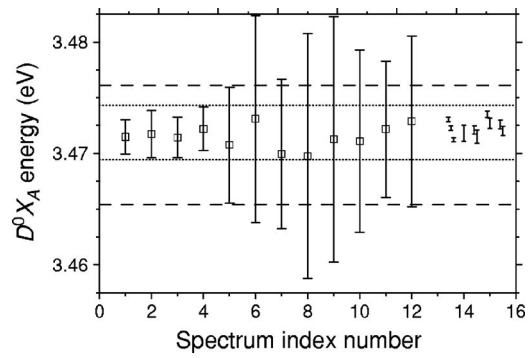

FIG. 5. Summary of curve-fitting results for the D^0X_A peak in low-temperature PL and CL spectra of GaN nanowire samples, and comparison with literature results for quasisubstrate samples. Each nanowire spectrum is identified by an index number (horizontal axis) as follows: (1) PL spectrum, sample B724, as-grown; (2) PL, sample B724, dispersed on sapphire; (3) PL, sample B724, polished; (4) PL, sample B738, as-grown; (5) PL, sample B738, dispersed on sapphire; (6) CL, sample B724, as-grown; (7) CL, sample B724, dispersed on stainless steel; (8) CL, sample B724, dispersed on AlGaAs; (9) CL, sample B724, polished; (10) CL, sample B738, as-grown; (11) CL, sample B738, dispersed on stainless steel; (12) CL, sample B738, dispersed on Si/Ti/Au. The peak energy, E_{peak}, is represented by a square symbol. Each peak is encompassed by a vertical bar from $E_{peak}-0.5W$ to $E_{peak}+0.5W$, where W is the full width at half maximum. Literature results for the D^0X_A peaks in freestanding quasisubstrate samples, from Refs. 19–23, are shown toward the right-hand edge of the graph. Each quasisubstrate peak is represented by a vertical bar from $E_{peak}-0.5W$ to $E_{peak}+0.5W$ (without a central symbol). The horizontal dashed and dotted lines represent exciton energy shifts (relative to the unstrained D^0X_A energy of 3.472 eV) calculated for particular c-axis strains in a hydrostatic stress model. The upper dashed line, upper dotted line, lower dotted line, and lower dashed line correspond, respectively, to $\varepsilon_{zz}=-1.6\times10^{-4}$ (compressive strain), $\varepsilon_{zz}=-9\times10^{-5}$ (compressive), $\varepsilon_{zz}=+1\times10^{-4}$ (tensile), and $\varepsilon_{zz}=+2.6\times10^{-4}$ (tensile).

The reason for the sample-to-sample variation in the strength of the free-exciton peaks (relative to the D^0X_A peak) is not known. When comparing the excitonic region PL spectra of different samples, it should be pointed out that the relative intensities and linewidths of the X_A and X_B peaks are known to vary with excitation intensity, which was difficult to ascertain in these measurements because of diffusion and scattering of the incident laser beam in the nanowire samples.

Room-temperature ($T\approx297$ K) PL and CL spectra of as-grown pieces of samples B724 and B738 are plotted in Figs. 7(a) and 7(b), respectively. The observed peaks are compared with the predicted room-temperature free-exciton (X_A) energy of 3.408 eV in unstrained GaN (calculated from the low-temperature X_A energy of 3.479 eV observed in quasisubstrates, and the Varshni parameters for the temperature dependence of the band gap recommended by Vurgaftman:[12] $\alpha=9.09\times10^{-4}$ eV/K, $\beta=830$ K). In sample B724, the PL and CL emission peaks are downshifted from the calculated X_A energy of 3.408 eV, with a slightly larger downshift for the CL peak. In addition, both peaks are broadened asymmetrically on the low-energy side. The room-temperature PL and CL emission peaks of sample B738 show increased broadening as compared to sample B724; the CL spectrum shows some fine structure, with a distinct peak at 3.373 eV and a high-energy shoulder near 3.408 eV, as indicated by the arrows in the figure. The downshift and asymmetric low-energy broadening of the room-temperature PL and CL spec-

Downloaded 20 Nov 2007 to 132.163.53.194. Redistribution subject to AIP license or copyright; see http://jap.aip.org/jap/copyright.jsp

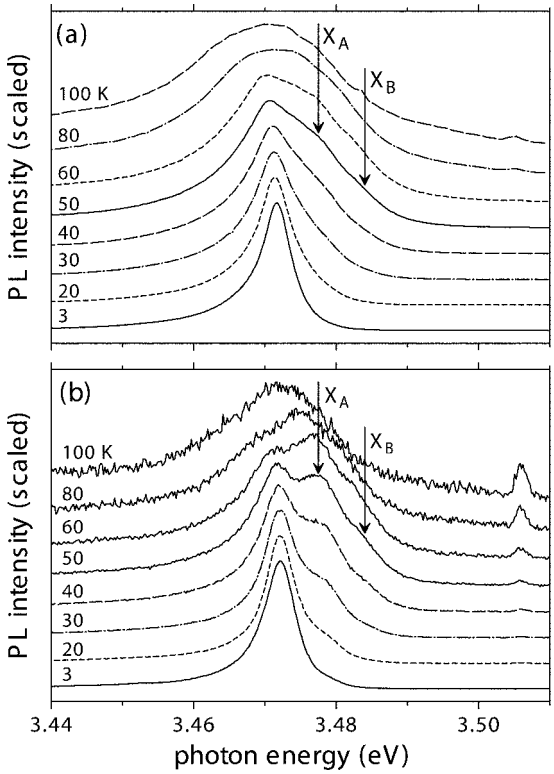

FIG. 6. Temperature dependence from 3 to 100 K of near-band-edge PL spectra of the following samples: (a) B724, dispersed on sapphire; (b) B738, as-grown. The X_A and X_B peak positions at intermediate temperature ($T \approx 50$ K) are indicated by vertical arrows.

tra may arise from a contribution of shallow band-tail states, with energies slightly below the free-exciton (X_A) energy, to the radiative recombination processes at room temperature. The origin of the band-tail states is not known.

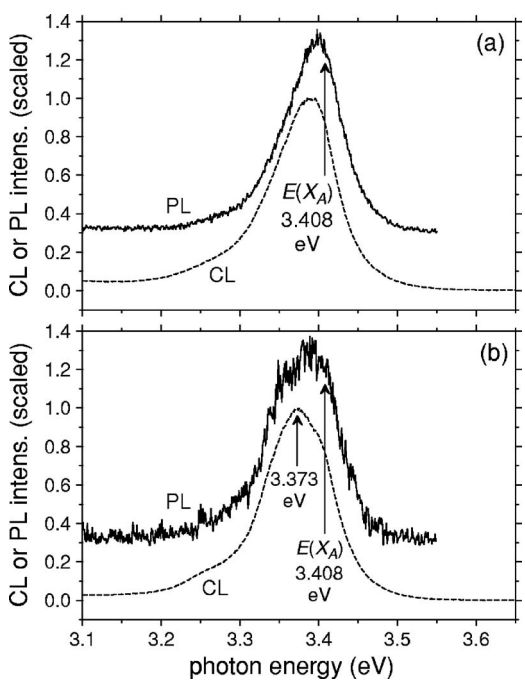

FIG. 7. Room-temperature ($T \approx 297$ K) PL (thin solid line) and CL (thick dashed line) spectra of (a) sample B724, as-grown; (b) sample B738, as-grown. Arrows indicate the calculated free-exciton (X_A) energy at room temperature (3.408 eV), and the observed CL emission peak of sample B738 (3.373 eV).

B. Lattice parameters and strain determination

Independent strain measurements are required to quantify strain effects on the optical properties. Accurate values of the lattice parameters of the strain-free wurtzite-structure GaN crystal, denoted (a_0, c_0), are required as inputs for strain determination from HRXRD measurements. Based on a recent HRXRD study of quasisubstrate GaN samples by Darakchieva *et al.*,[24] the room-temperature values of (a_0, c_0) are estimated as $a_0 = 0.318\,915(30)$ nm and $c_0 = 0.518\,531(14)$ nm (averages of the reported measurements[24] from the top surfaces of four samples). The values of Darakchieva *et al.*[24] were accepted as working estimates of (a_0, c_0) for the following results: first, all samples were freestanding single crystals with low defect and impurity content (as shown by several independent measurements); second, good agreement was found between the measured lattice parameters of samples with thicknesses from 30 to 380 μm; finally, sources of error in the lattice parameter determination were minimized by careful HRXRD alignment and correction procedures.[28]

Lattice parameters similar to Darakchieva *et al.*[24] were reported in other studies of high-quality GaN samples. In particular, Leszczynski *et al.*[29] estimated $a_0 = 0.318\,85$ nm, $c_0 = 0.518\,50$ nm (uncertainties not stated) from analysis of a "broad spectrum of samples" including single-crystal platelets, homoepitaxial and heteroepitaxial films; Torii *et al.*[30] reported $a = 0.318\,98(2)$ nm, $c = 0.51855(2)$ nm from Bond method XRD analysis of a 70 μm freestanding layer; Paskowicz *et al.*[31] reported $a = 0.318\,940(1)$ nm, $c = 0.518\,614(2)$ nm from Rietveld refinement analysis of a powder sample (with ≈ 6 μm particle diameter); and, room-temperature ($T = 297$ K) lattice parameters $a = 0.318\,93$ nm, $c = 0.518\,51$ nm can be deduced from the thermal expansion data of Roder *et al.*[32] for a 326 μm thick quasisubstrate layer ("sample C" in that study). The fractional differences between the lattice parameters reported by Leszczynski,[29] Torii,[30] Paskowicz,[31] or Roder,[32] and those of Darakchieva,[24] are seen to be less than 2×10^{-4}. [Lattice parameter values $a_0 = 0.318\,76$ nm, $c_0 = 0.518\,46$ nm (uncertainties not stated), based on an XRD study by Porowski[33] of a homoepitaxial film on a Mg-doped platelet, are also sometimes cited. These values, especially a_0, appear to be outliers compared to the results of the other cited studies of high crystalline quality GaN; further, few details on sample preparation or XRD measurement procedure are given in Porowski.[33]]

Table II shows a and c for samples B724 and B738, determined by HRXRD as reported previously.[15] In addition, Table II shows the calculated strains based on the estimates $a_0 = 0.318\,915(30)$nm, $c_0 = 0.518\,531(14)$ nm for the unstrained lattice parameters. The calculated strains in the nanowires (resolved from the matrix layer) within sample B724, and in the nanowires+matrix layer (unresolved) in sample B738, are less than the measurement uncertainty. Significant strain is found in the matrix layer in sample B724; the form of this strain ($\varepsilon_a > 0$, $\varepsilon_c / < 0$, $\varepsilon_c / \varepsilon_a = -0.38$) suggests tensile biaxial stress in the basal (0001) plane.

Downloaded 20 Nov 2007 to 132.163.53.194. Redistribution subject to AIP license or copyright; see http://jap.aip.org/jap/copyright.jsp

TABLE II. Room-temperature lattice parameters (a,c) of GaN nanowire samples B724 and B738 from high-resolution x-ray diffraction, and strains $(\varepsilon_a,\varepsilon_c)$ based on unstrained lattice parameters from Ref. 24: a_0 =0.318 915(30) nm, c_0=0.518 531(14) nm. Uncertainties in the least significant digits (which represent 2σ error bars) are shown in parentheses.

Sample	a (nm)	c (nm)	ε_a	ε_c
B724, nanowires (resolved from matrix layer)	0.318930(100)	0.518530(50)	0.00005(33)	0.00000(10)
B724, matrix layer	0.319240(100)	0.518330(50)	0.00102(33)	−0.00039(10)
B738 (primarily nanowires with unresolved matrix layer contribution)	0.318980(100)	0.518460(50)	0.00020(33)	−0.00014(10)

IV. DISCUSSION

Key characterization results for the GaN nanowire samples are summarized as follows. Low-temperature PL spectra showed a D^0X_A emission peak at essentially the same energy as observed in quasisubstrate samples of high crystalline quality, but with larger full width at half maximum (W =3.1 meV to W=10.4 meV, with median value W=4 meV for five PL spectra). In addition, the PL spectra showed asymmetric broadening on the low-energy side of the D^0X_A peak, which was treated empirically in the curve-fitting analysis by introducing a lower-energy L peak of unknown physical origin. The full width of the D^0X_A peak was significantly larger in low-temperature CL spectra (W=12 meV to W=22 meV, with median value W=16 meV for seven CL spectra) than in PL spectra of the same nanowire samples. Free-exciton (X_A and X_B) peaks were observed in PL spectra in the 30–80 K range. HRXRD lattice parameter measurements showed low strain in the nanowires.

We suggest that the observed broadening of the low-temperature, near-band-edge PL peaks in the nanowires (as compared to quasisubstrate samples) may be caused by inhomogeneous residual strain, possibly arising from strain fields of structural defects such as dislocations or twin boundaries, or thermally induced stress due to thermal expansion mismatch between the nanowire and substrate. Strain effects on the exciton energies are quantified by parameters called the electronic deformation potentials. The following analysis is based on the deformation potentials of Gil[34] and Alemu (for the A exciton in wurtzite-structure GaN), given by the equation

$$\Delta E_A = (-15.55\varepsilon_a - 10.23\varepsilon_c)\ \text{eV}, \tag{1}$$

(where ΔE_A is the strain shift of the exciton energy), and the elastic constants of Yamaguchi,[35] which were obtained from a Brillouin scattering study. (The deformation potentials of Gil[34] are partially based on the elastic constants of Yamaguchi,[35] and hence should be used with these elastic constants for consistency.) The measured shifts of the exciton peaks of GaN with hydrostatic stress[36,37] and residual, c-plane stress[38] agree well with the parameters of Gil[34] and Yamaguchi.[35] Other researchers have reported somewhat different values for the electronic deformation potentials of GaN, as discussed in Ref. 12; the use of different deformation potentials would not significantly affect our analysis.

The strain shift ΔE_A can be calculated from Eq. (1) for various stress models. For hydrostatic (fully isotropic) stress σ_H, the result is $\Delta E_A=-(0.0422\ \text{eV/GPa})\sigma_H=-(25.5\ \text{eV})\varepsilon_c$; for equibiaxial stress $\sigma_{xx}=\sigma_{yy}$ in the c-plane (typical of c-plane films on mismatched substrates), the result is $\Delta E_A =-(0.0218\ \text{eV/GPa})\sigma_{xx}=+(15.8\ \text{eV})\varepsilon_c$; and, for uniaxial stress σ_c along the c-axis (which might occur, for example, in a nanowire with stressors at the ends of the wire), the result is $\Delta E_A=-(0.0203\ \text{eV/GPa})\sigma_c=-(6.68\ \text{eV})\varepsilon_c$.

The horizontal dashed lines in Fig. 5 represent the upper and lower limits of a hypothetical strain distribution that encompasses the full width at half maximum range ($E_{\text{peak}}-0.5W$ to $E_{\text{peak}}+0.5W$) of the fitted D^0X_A lines in the low-temperature PL spectra of the nanowire samples. The upper dashed line shows ΔE_A for c-axis strain of $\varepsilon_c=-1.6\times10^{-4}$, and the lower dashed line shows ΔE_A for c-axis strain of $\varepsilon_c=+2.6\times10^{-4}$, in a hydrostatic stress model.

In addition, the horizontal dotted lines in Fig. 5 represent the limits of a smaller strain distribution than encompasses the full width range of the fitted D^0X_A lines in the PL spectra of four nanowire samples (excluding sample B738 dispersed on sapphire, which shows a significantly larger PL linewidth than the other samples). The upper dotted line shows D^0X_A for c-axis strain of $\varepsilon_c=-9\times10^{-5}$, and the lower dotted line shows D^0X_A for c-axis strain of $\varepsilon_c=+1.0\times10^{-4}$, in a hydrostatic stress model.

The magnitudes of the above strain distributions are comparable to the uncertainties of the strain in the nanowires as measured by HRXRD (Table II). Note that larger strains would be required to produce the same energy shifts for uniaxial stress along the c-axis, because of the smaller strain shift coefficient for uniaxial stress ($\partial E_A/\partial\varepsilon_c=-6.68$ eV) than for hydrostatic stress ($\partial E_A/\partial\varepsilon_c=-25.5$ eV).

We next consider the additional, large broadening of the D^0X_A peak in the low-temperature CL spectra (as compared to PL spectra of the same samples). One possible mechanism for differing PL and CL line shapes is different excitation volumes within an inhomogeneous sample. However, the penetration depth of the 3.813 eV incident photons in PL is estimated to be 90 nm, while the range of the 3.14 keV incident electrons in CL is estimated to be 48 nm; the effective excitation volumes are probably further increased by carrier and exciton diffusion effects. It thus appears unlikely that the line shape difference between PL and CL arises from

Downloaded 20 Nov 2007 to 132.163.53.194. Redistribution subject to AIP license or copyright; see http://jap.aip.org/jap/copyright.jsp

different excitation volumes. We suggest instead that the additional broadening of the CL peaks is Stark effect broadening induced by the electric fields of charges created in the CL excitation process, and trapped at or near the surfaces of the nanowires. Surface charging effects are known to be common[26] in CL-SEM, especially because of the high beam currents typically used, e.g., 21.5 nA in this study. In addition, the surface charge Stark effects are expected to be stronger in nanowires than in planar films because of the high surface-area-to-volume ratio.

When considering a possible surface charge contribution to the luminescence line shape, it should be pointed out that surface charging may also occur in PL (i.e., photogenerated carriers may be trapped at or near the surface); hence, surface charge effects may contribute to the broadening of the PL peaks in the nanowires, although to a lesser extent than in CL.

V. CONCLUSIONS

Radiative recombination in as-grown and dispersed GaN nanowire samples, grown by plasma-assisted MBE, was studied by PL and CL spectroscopy at temperatures from 3 to 297 K. In addition, the lattice parameters of as-grown nanowires were measured by HRXRD at room temperature. The lattice parameters of the nanowires are in good agreement with recent measurements of freestanding "quasisubstrates," which suggests low average strain ($\leq 2\times 10^{-4}$) in the nanowires. The low-temperature (3–15 K) PL and CL spectra of the nanowires were dominated by the recombination of excitons bound to neutral, shallow donor impurities (D^0X_A centers, $\approx$3.472 eV). Free-exciton peaks (X_A at $\approx$3.479 eV, and X_B at $\approx$3.484 eV) were resolved in PL spectra at temperatures between 20 and 80 K. The full width at half maximum, W, of the D^0X_A peak was broader in low-temperature PL spectra of nanowires than quasisubstrates. The broadening of the D^0X_A peak in the nanowires is tentatively ascribed to inhomogeneous stress/strain. The fitted full width at half maximum, W, of the D^0X_A peak was significantly larger in low-temperature CL spectra than in low-temperature PL spectra of the same nanowire samples (the median value of W for several CL spectra was 16 meV, while the median value of W for several PL spectra was 4 meV). The further broadening of the D^0X_A peak in CL is tentatively ascribed to Stark effect broadening induced by the electric fields of trapped charges, which are created in the CL excitation process.

ACKNOWLEDGMENT

We wish to acknowledge Igor Levin for providing the TEM data and for helpful discussions.

[1] M. Law, J. Goldberger, and P. Yang, Annu. Rev. Mater. Res. **34**, 83 (2004).
[2] F. Qian, Y. Li, S. Gradecak, D. Wang, C. J. Barrelet, and C. M. Lieber, Nano Lett. **4**, 1975 (2004).
[3] F. Qian, S. Gradecak, Y. Li, C. Y. Wen, and C. M. Lieber, Nano Lett. **5**, 2287 (2005).
[4] S. Gradečak, F. Qian, Y. Li, H. G. Park, and C. M. Lieber, Appl. Phys. Lett. **87**, 173111 (2005).
[5] E. Calleja, M. A. Sanchez-Garcıa, F. J. Sanchez, F. Calle, F. B. Naranjo, E. Munoz, U. Jahn, and K. Ploog, Phys. Rev. B **62**, 16826 (2000).
[6] Y. S. Park, C. M. Park, D. J. Fu, T. W. Kang, and J. E. Oh, Appl. Phys. Lett. **85**, 5718 (2004).
[7] X. Duan and C. M. Lieber, J. Am. Chem. Soc. **122**, 188 (2000).
[8] L. Dai, S. F. Liu, L. P. You, J. C. Zhang, and G. G. Qin, J. Phys.: Condens. Matter **17**, L445 (2005).
[9] B. Ha, S. H. Seo, J. H. Cho, C. S. Yoon, J. Yoo, G. C. Yi, C. Y. Park, and C. J. Lee, J. Phys. Chem. B **109**, 11095 (2005).
[10] M. Kang, J. S. Lee, S. K. Sim, H. Kim, B. Min, K. Cho, G. T. Kim, M. Y. Sun, S. Kim, and H. S. Han, Jpn. J. Appl. Phys., Part 1 **43**, 6868 (2004).
[11] S. C. Jain, M. Willander, J. Narayan, and R. Van Overstraeten, J. Appl. Phys. **87**, 965 (2000).
[12] I. Vurgaftman and J. R. Meyer, J. Appl. Phys. **94**, 3675 (2003).
[13] M. A. Reshchikov and H. Morkoc, J. Appl. Phys. **97**, 061301 (2005).
[14] K. A. Bertness, N. A. Sanford, J. M. Barker, J. B. Schlager, A. Roshko, A. V. Davydov, and I. Levin, J. Electron. Mater. **35**, 576 (2006).
[15] K. A. Bertness, J. B. Schlager, N. A. Sanford, A. Roshko, T. E. Harvey, A. V. Davydov, I. Levin, M. D. Vaudin, J. M. Barker, P. T. Blanchard, and L. H. Robins, "High Degree of Crystalline Perfection in Spontaneously Grown GaN Nanowires," in *GaN, AlN, InN and Related Materials*, MRS Symposium Proceeding 892, edited by M. Kuball, T. H. Myers, J. M. Redwing, and T. Mukai (Materials Research Society, Warrendale, PA, 2006).
[16] K. A. Bertness, A. Roshko, N. A. Sanford, J. M. Barker, and A. V. Davydov, J. Cryst. Growth **287**, 522 (2006).
[17] L. H. Robins, K. A. Bertness, J. M. Barker, N. A. Sanford, and J. B. Schlager, J. Appl. Phys. **101**, 113506 (2007), following article.
[18] N. A. Sanford, L. H. Robins, M. H. Gray, Y.-S. Kang, J. E. Van Nostrand, C. Stutz, R. Cortez, A. V. Davydov, A. Shapiro, I. Levin, and A. Roshko, Phys. Status Solidi C **2**, 2357 (2005).
[19] D. C. Look, Z. Q. Fang, and B. Claflin, J. Cryst. Growth **281**, 143 (2005).
[20] D. Gogova, A. Kasic, H. Larsson, B. Pecz, R. Yakimova, B. Magnusson, B. Monemar, F. Tuomisto, K. Saarinen, C. Miskys, M. Stutzmann, C. Bundesmann, and M. Schubert, Jpn. J. Appl. Phys., Part 1 **43**, 1264 (2004).
[21] D. Gogova, A. Kasic, H. Larsson, C. Hemmingsson, B. Monemar, F. Tuomisto, K. Saarinen, L. Dobos, B. Pecz, P. Gibart, and B. Beamont, J. Appl. Phys. **96**, 799 (2004).
[22] D. Gogova, H. Larsson, A. Kasic, G. R. Yazdi, I. Ivanov, R. Yakimova, B. Monemar, E. Aujol, E. Frayssinet, J. P. Faurie, B. Beaumont, and P. Gibart, Jpn. J. Appl. Phys., Part 1 **44**, 1181 (2005).
[23] D. Gogova, E. Talik, I. G. Ivanov, and B. Monemar, Physica B (Amsterdam) **371**, 133 (2006).
[24] V. Darakchieva, T. Paskova, P. P. Paskov, B. Monemar, N. Ashkenov, and M. Schubert, J. Appl. Phys. **97**, 013517 (2005).
[25] T. E. Everhart and P. H. Hoff, J. Appl. Phys. **42**, 5837 (1971).
[26] A. Gustafsson, M.-E. Pistol, L. Montelius, and L. Samuelson, J. Appl. Phys. **84**, 1715 (1998).
[27] J. B. Schlager, N. A. Sanford, K. A. Bertness, J. M. Barker, A. Roshko, and P. T. Blanchard, Appl. Phys. Lett. **88**, 213106 (2006).
[28] P. F. Fewster and N. L. Andrew, J. Appl. Crystallogr. **28**, 451 (1995).
[29] M. Leszczynski, P. Prystawko, T. Suski, B. Lucznik, J. Domagala, J. Bakmisuik, A. Stonert, A. Turos, R. Langer, and A. Barski, J. Alloys Compd. **286**, 271 (1999).
[30] K. Torii, T. Deguchi, T. Sota, K. Suzuki, S. Chichibu, and S. Nakamura, Phys. Rev. B **60**, 4723 (1999).
[31] W. Paszkowicz, S. Podsiadlo, and R. Minikayev, J. Alloys Compd. **382**, 100 (2004).
[32] C. Roder, S. Einfeldt, S. Figge, and D. Hommel, Phys. Rev. B **72**, 085218 (2005).
[33] S. Porowski, J. Cryst. Growth **189–190**, 153 (1998).
[34] B. Gil and A. Alemu, Phys. Rev. B **56**, 12446 (1997).
[35] M. Yamaguchi, T. Yagi, T. Azuhata, T. Sota, K. Suzuki, S. Chichibu, and S. Nakamura, J. Phys.: Condens. Matter **9**, 241 (1997).
[36] Z. X. Liu, S. Pau, K. Syassen, J. Kuhl, and W. Kim, Phys. Rev. B **58**, 6696 (1998).
[37] K. Reimann, M. Steube, O. Brandt, H. Yang, and K. H. Ploog, J. Appl. Phys. **84**, 2971 (1998).
[38] C. Kisielowski, J. Kruger, S. Ruvimov, T. Suski, J. W. Ager III, E. Jones, Z. Liliental-Weber, M. Rubin, and E. R. Weber, Phys. Rev. B **54**, 17745 (1996).

Downloaded 20 Nov 2007 to 132.163.53.194. Redistribution subject to AIP license or copyright; see http://jap.aip.org/jap/copyright.jsp